Chapter 13
Nanoaerosol

Nanomaterials are now widely used in many industries, for example, for improving combustion efficiency, environmental protection, health, and renewable energy production. Once these nanoparticles enter the air, they may result in nano air pollution and have to be monitored and filtered for the protection of the environment and health. Engineering approaches to nano air pollution control is the core part of this chapter. Specially, it will cover the properties of nano air pollution and its implications on air monitoring and air filtration technologies.

13.1 Sources of Nanoaerosol

Nanoaerosols are nanoparticles suspended in a gas. These nanoparticles could be liquid droplets but more often solid particles with at least one dimension being less than 100 nm. Most researchers consider nanoaerosol as another name of ultrafine aerosol or ultrafine particulate matter. There is actually a slight difference between ultrafine aerosol or particulate matter and nanoaerosol. The former is commonly used to describe airborne nanoparticles that are produced incidentally without intension and are suspended in the atmosphere. The latter has a broader coverage including both environmental and engineered nanoparticles in any carrier gas.

Nanoaerosols are produced from various sources intentionally or as a byproduct. Environmental nanoaerosols are produced in the atmosphere by natural nucleation and condensation or incomplete combustion of hydrocarbons. The latter are mostly soot particles; a soot particle is a cluster of nanoparticles between 10 and 100 nm. Engineered nanoaerosols are a result of recent rapid advances in nanotechnology, produced when manufactured nanomaterials become suspended in the air or other carrier gases. These particles usually have complex shapes including sphere, cube, cylinder, flake, crystal, and so on. As introduced in Chap. 4, these different shapes affect their aerodynamics.

Thousands of years ago, the Chinese started collecting soot particles from burnt pine to make high quality ink for fine painting. This may be the earliest engineered nanoaerosol. Nowadays, engineered nanomaterials find more applications to the

Z. Tan, *Air Pollution and Greenhouse Gases*, Green Energy and Technology,
DOI 10.1007/978-981-287-212-8_13

improvement of our quality of life. Many different types of nanosized drugs have been developed and some of them can be aerosolized and delivered by inhalation. Respiratory nanomedicine delivery benefits a patient due to high drug deposition in central and peripheral regions of the lungs [7]. However, human respiratory systems did not seem to be effective in capturing nanoaerosol particles smaller than 40 nm [23]. Drug delivery systems for nanoaerosol are believed to have potential to significantly reduce extrathoracic depositional drug loss [7]. Dosing effect can be improved by charging the particles. Manufacturing cylindrical or tubular shaped nanoaerosol drugs may also help since their actual aerodynamic diameters are increased to micron range and tend to travel only one way into the human respiratory system. On the other hand, manufacturing sub-10 nanoaerosol-based drugs and associated delivery devices are challenging because they agglomerate easily at high concentrations.

Another example is the wide use of nano-silver spray as a disinfectant. During the short life of nanoaerosol after spraying, high dose exposure could result in acute or chronic health effects. The mechanisms of toxicity of silver ions (Ag^+) are well known, but little is known about toxicity nano-silver induced to living organisms. In addition, limited data available has shown that other potentially hazardous and toxic materials are involved in the product and the disinfectant spray could also have negative impacts on the environment and human health.

Nanotechnology market keeps increasing in the past decade to a level of the order of hundreds billion US dollars, according to a report of European Agency for Safety and Health at Work [5]. New market opportunities lead to growing concerns regarding potential risks to the environment and health of human beings. In addition to the safety risk of explosion, some experts suspect that nanomaterials affect health more than microscale materials. At the workplace, workers can be exposed during the production process, use of nanomaterials, transport, storage or waste treatment.

Nanomaterials might also have negative impact on the environment by water and solid contamination, causing indirect impact on people's health. As illustrated in Fig. 13.1, nanoaerosol emitted and formed in the atmosphere eventually falls down to the ground with precipitation. Many experts in nanotechnology believe that it is the next industrial revolution. On the other hand, new technologies come with new risks, which are discovered often later than their benefits.

13.2 Exposure to Nanoaerosol

While the society is enjoying the benefits and excitement brought by nanotechnology, some experts are concerned about its negative impact on human health and the environment. In addition to the nanoaerosol produced in nature and by combustion, recent rapid advances in nanotechnology have outpaced the risk assessment and government regulations in this industry. Nanoaerosol can be more toxic than larger ones of the same material because of their small size, large surface area and great diffusivity. Long-term exposure to nanoaerosol may cause ischemic heart disease, cardiovascular diseases, stroke, chronic bronchitis, asthma, and respiratory tract infections [14].

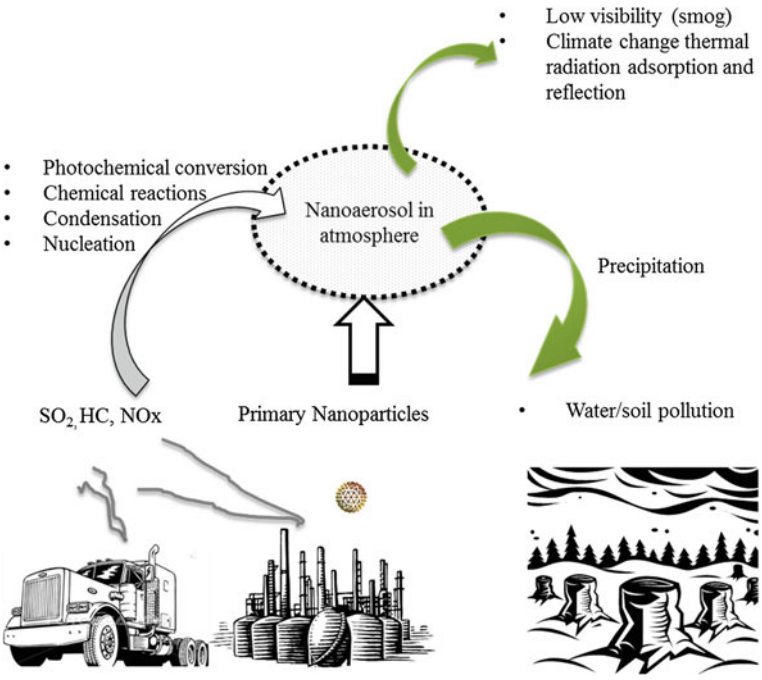

Fig. 13.1 Environmental impact of nanoaerosol

Nanoparticles in certain size range can transport toxic chemicals into the human body through the respiratory system. These chemicals may cause more damage than their counterparts in micron size range. Comparison between the rat's exposure to 250 and 20 nm titanium oxide (TiO_2) aerosol particles of the same weight showed that more 20 nm particles were trapped in the lung, resulting in inflammation [12]. Similar studies showed that exposure to 30-nm Teflon particles, which are considered as inert at micron level, led to acute pulmonary toxicity in rats [27].

Nanoparticles can cause adverse health effects due to the direct action of the particles or to their rate as carriers of toxic elements [61]. Because nanoparticles are not removed from the upper respiratory tract, they are inhaled into the deeper areas. Their rather high deposition (more than 90 %) in the alveolar region or other respiratory tract regions leads to their subsequent entry into the blood stream [7, 58]. The small size and large surface area of nanoparticles enable significant interaction with biological systems. Nanoaerosols may also cause toxic effects on other organs. Nanoaerosols deposited in alveolar region or other respiratory tract region can lead to diffusion into the circulatory system [58], and they can reach the brain and the heart. A direct interaction of particles (or compounds generated by particles) with DNA is considered possible. Therefore, there may be a great risk of carcinogenicity.

The most important toxic effects are induced by nanoaerosol inhalation, and thereby chronic toxicity and carcinogenicity in the lungs [39]. Since the size of nanoaerosol particles is smaller than cells, they can penetrate through the respiratory

or integumentary system and leach into the bloodstream. Contrary to neutral nanoaerosols of the same size; charged nanoaerosol particles have a much greater probability of depositing into the lungs [9]. Similar to the effects of fine aerosol, nanoaerosol can cause inflammation, fibrosis, and lung tumors if the exposure at workplaces passes certain threshold and long-lasting. Increased surface area and decreased particle diameter are believed to be the cause of the increased toxicity of granular nanomaterials in the lungs. Lung toxicity, evidenced by inflammation and tissue damage, was also proven to be induced by fibrous nanomaterials such as carbon nanotubes (CNTs). Despite of the evidences provided by tests using rate, mice, and hamsters, not everybody agrees with the mechanisms of tumor development.

Effects on the skin or a relevant skin penetration were not well quantified. However, the barrier function of the skin could be breached by the presence of skin lesions, strong mechanical strain or small-sized nanoparticles (<5–10 nm). For example, a human case of allergic response to nanomaterials was described by a person exposed to dendrimers in Japan [57]. A 22-year old student involved in synthesis of dendrimers developed erythema multiforme-like contact dermatitis on his hands. Conventional treatments and anti-histamines could not stop the disease from progressing to other areas of the body. After 3 weeks of hospitalization, he recovered, but it appeared again when he reentered the same laboratory.

At this moment, there is no legal standard that sets the occupational exposure threshold of nanoaerosol. The development of risk assessment of exposure to nanoaerosol has been limited by the lack of standard methods and compact instrumentation for long term monitoring. Accurate risk assessment requires advanced nanoaerosol sampling and characterization techniques for the analysis of both physical and chemical properties of nanoaerosol. Nonetheless, occupational exposure limits for nanomaterials are set by different organizations. Proposed occupational exposure limits for engineered nanoaerosol are summarized in Table 13.1.

Table 13.1 Proposed occupational exposure limits of nanoaerosols

Nanoaerosol	Occupational exposure limit	Parameters
Titanium dioxide	0.1 mg/m^3	0.1 risk level particles\100 nm
General dust	3 mg/m^3	
Photocopier toner	0.6 mg/m^3	Tolerable risk
	0.06 mg/m^3	2009 acceptable risk
	0.006 mg/m^3	2018 acceptable risk
Biopersistent granular materials (e.g., metal oxides)	20,000 particles/cm^3	Density > 6,000 kg/m^3
	40,000 particles/cm^3	Density < 6,000 kg/m^3
Carbon Nanotubes (CNTs)	0.01 f/cm^3	Exposure risk ratio for asbestos
Fibrous	0.01 f/cm^3	3:1; length 75,000 nm
Multi-walled CNTs	0.0025 mg/m^3	Nanocyl product only [40]

Source Schulte et al. [47]

13.3 Properties of Nanoaerosol

13.3.1 Number and Size of Nanoaerosol Particles

As shown Fig. 13.2, by number, nanoaerosol particles constitute 90 % or more of ambient aerosols, although they only account for a very small fraction of the total mass [48].

The small size of nanoparticles leads to a great surface area to mass ratio and consequently other unique properties of nanoparticles. The high surface area leads to a great surface reactivity. On a nano scale, both classic physics and quantum physics play roles in the interfacial behavior of nanoaerosols.

Some researchers believe that high concentration nanoparticles in the air agglomerate rapidly to form larger particles by chemical bonding and physical reactions [51]. As a result, the lifespan of individual nanoaerosol particles is usually short. Nanoparticles with the sizes of 1–10 nm have the lifespan of a few minutes to hours [2]. Meanwhile larger nanoparticles are formed by agglomeration. As a result, the size distribution of the nanoaerosol in a certain environment may change over time. The agglomeration mechanisms of nanoaerosols are not yet well understood.

On the other hand, well-dispersed nanoaerosols at low concentration may remain airborne for a long period of time; their setting velocity is extremely low because of their small aerodynamic sizes. At low concentration, the chance for nanoaerosol particles to agglomerate is low because of their great impact velocities.

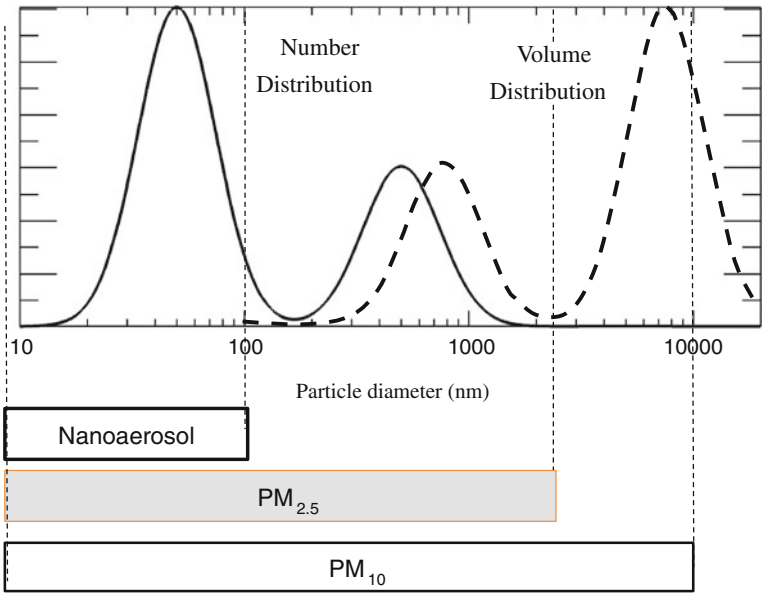

Fig. 13.2 Aerosol number and mass distribution versus size

To take advantage of the unique properties of nanoaerosol, one of the future trends in nanomedicine is targeted drug delivery to the respiratory system by nanoaerosol; it is important to improvement of drug therapies, lung imaging, gene delivery and therapy, tuberculosis diagnosis and treatment. It is important to clearly understand the toxicological effect of inhaled nanoaerosol to address the increasing concerns over potentially harmful public and occupational exposure. And this type of research should be conducted systematically on a global scale.

13.3.2 Noncontinuum Behavior

Nanoaerosol particles are small enough to approach the mean free path of air, which is about 67 nm under standard conditions. For nanoaerosol the continuum assumption is no longer valid and can attain free molecular flow; there is a non-continuum interaction between the particles and the carrier gas. The dimensionless parameter that defines the nature of the aerosol is the Knudsen number, which is the ratio of gas mean free path to particle radius.

$$Kn = 2\lambda/d_p \tag{13.1}$$

where d_p is the particle diameter and λ is the gas mean free path that was introduced in Sect. 2.1.7 above. Under normal conditions the mean free path of the air molecules is 66 nm. Thereby Kn is in the range of 1.32–132 when the diameter of nanoparticle drops from 100 to 1 nm. Now the air-nanoparticle is in noncontinuum regime, Cunningham correction factor, C_c, becomes much more important than micro sized particles.

$$C_c = 1 + Kn\left[1.142 + 0.558\exp\left(-\frac{0.999}{Kn}\right)\right] \tag{13.2}$$

Both Kn and C_c are dimensionless parameters. Since the theoretical value of C_c is always greater than 1, the drag force experienced with slipping effect considered is always smaller than the value calculated with non-slipping assumption. The drag force exerted by the air on the nanoaerosol is calculated by

$$F_D = \frac{3\pi\mu\left(V_p - V_g\right)d_p}{C_c} \tag{13.3}$$

Under normal conditions, air flow immediately surrounding a nanoaerosol particle is laminar or in the Stokes regime, although the bulk air flow may be turbulent. In addition, a nanoaerosol particle tends to follow the moving carrier gas and it is very difficult to separate them simply by inertia.

13.3.3 Diffusion of Neutral Nanoaerosol

The diffusion coefficient of uncharged nanoaerosol particles in the air can be determined by the Stokes-Einstein equation described in Eq. (13.4):

$$D_p = \frac{kTC_c}{3\pi\mu d_p} \tag{13.4}$$

where k is the Boltzmann's constant, T the temperature, μ the kinetic viscosity of the carrier gas. For smaller nanoparticles in the size range of 0.5–2 nm, the diffusivity can be calculated using the equation given by Ichitsubo et al. [21] as

$$D_p = \frac{0.815 c_{\text{rms}}}{12\pi N\left(d_g + d_p\right)^2}\sqrt{1+\frac{M}{M_n}} \tag{13.5}$$

where d_g is the gas molecule diameter (0.37 nm for air), N is the number concentration of gas molecules ($2.45 \times 10^{25}/\text{m}^3$ for air at 293 K and 1 atm), M is the molar weight of the carrier gas (28.82 for air), M_n is the molar weight of nanoaerosol particles, c_{rms} is the root mean square velocity of the carrier gas molecules, which can be determined using Eq. (13.6).

$$c_{\text{rms}} = \left(\frac{3RT}{M}\right)^{1/2} \tag{13.6}$$

13.3.4 Electrical Properties of Nanoaerosol

Nanoaerosol particles are primarily charged by diffusive charging. The number of ions charged to a nanoaerosol particle is calculated using Eq. (13.7) [63]

$$n(t) = \frac{d_p kT}{2e^2 K_E}\ln\left(1+\frac{d_p K_E \bar{c}_i \pi e^2 N_{i0}}{2kT}t\right) \tag{13.7}$$

where $\bar{c}_i$ is the mean thermal speed of ions (239 m/s at standard conditions $T = 293$ K, $P = 1$ atm), k is Boltzmann constant (1.38×10^{-23} J/K), K_E is a constant of proportionality ($1/4\pi\varepsilon_0 = 9 \times 10^9$ Nm^2/C^2), N_{i0} is ion concentration.

While micron particles may be charged with hundreds of ions, a nanoaerosol particle smaller than 20 nm will probably acquire only a couple of ions; in some cases it will not acquire any. If polydisperse nanoaerosol particles pass through a bipolar charger, two nanoparticles of the same size may obtain different charges [32]. Experimental data show that generally, after charging, sub-20 nm particles carry a negative charge while larger particles carry a positive charge [1].

High concentration of ions and sufficient charging time allow particles to reach maximum charging. The maximum charging by unipolar charging enables the

particles to carry ions with same polarity, negative or positive. Charged particles are subjected to electrical forces in an electrical field. The bipolar charging process eventually leads to Boltzmann charge equilibrium if the particles experience sufficient charging time. In such cases, they are considered neutralized. Highly charged particles may be discharged by colliding with ions with different polarity [43].

There are many types of nanoaerosol chargers. Unipolar ions can be produced by unipolar corona discharge, UV charging, carbon fiber ionizer, and separation of ions produced by bipolar ions. Bipolar ions are usually produced by radioactive sources such as Kr^{85} or Po^{210}, soft X-ray, AC corona discharge or dual electrode corona discharge. According to the mechanisms of ion generation, the chargers can be classified into:

- Corona discharge chargers,
- Radioactive chargers, and
- Photoelectric chargers.

Corona discharge is the most commonly used for high ion concentrations [22]. Bipolar charging method has a lower charging efficiency due to particle loss and ions recombination. In the unipolar method, produced ions in the corona charger are moved using the filtered air passing opposite the aerosol flow. Filtered air causes aerosols to be diluted and decreases charging efficiency.

However, nanoparticles may be generated in a corona. Various studies have investigated nanoparticle generation associated with bipolar and unipolar corona chargers [26, 35, 45, 52] and have reported methods to reduce nanoparticle generation in corona charging. One reason for generating nanoparticles by the corona charger is that a corona charger has enough energy to start gas-phase chemical reactions in the charger region, such as forming ozone from oxygen, which may lead to particle generation [45]. Moreover, sputtering of metal from the surface or erosion of the electrodes is another reason which may cause particles to be generated [30].

13.4 Separation of Nanoaerosol from the Air

Separation of general aerosol particles and particulate matter has been introduced in Chap. 6. Among the technologies introduced therein, separation based on inertia in cyclone and gravity settling chamber have almost no effect on nanosized size range. Under normal conditions, nanoaerosol particles follow the air due to their non-continuum behavior.

It is technically challenging to remove nanoparticles from the air by electrostatic precipitators (ESPs) only because nanoaerosol particle charging efficiency is low. Furthermore, extra nanoaerosol particles are likely to be produced in corona chargers, which is a critical component of an ESP. Passing nanoaerosol through a liquid (e.g., water) column can effectively remove the unwanted particles from the

air. It may work effective for small quantity of air, however, it becomes costly for large air flow rates.

Filtration of nanoaerosol particles from its carrier gas is important to nanoaerosol sampling and characterization as well as air cleaning. The filtration efficiency for nanoaerosol is also described using Eq. (13.8)

$$\eta_{\text{nano}} = \eta_{\text{ts}}\eta_{\text{ad}} \tag{13.8}$$

13.4.1 Nanoparticle Transport Efficiency

Same as microparticles, nanoparticle transport efficiency (η_{ts}) is calculated based on the single fiber efficiency (η_{sf}) as described in Sect. 6.5:

$$\eta_{\text{ts}} = 1 - \exp\left[\frac{-4\alpha\eta_{\text{sf}}L}{(1-\alpha)\pi d_f}\right] \tag{13.9}$$

where d_f is the diameter of the fiber, L is the thickness of the bulk filter, and α is the solidity of the filter. The single fiber filtration efficiency can still be determined using Eq. (6.8)

$$\eta_{\text{sf}} = 1 - (1-\eta_{\text{it}})\left(1-\eta_{\text{ip}}\right)(1-\eta_D)(1-\eta_E) \tag{13.10}$$

However, the dominating mechanisms for removing neutral airborne nanoparticles using fibrous filters are Brownian diffusion and interception.

$$\eta_{\text{sf}} = 1 - (1-\eta_{\text{it}})(1-\eta_D) \tag{13.11}$$

There have been several models developed for these mechanisms, and the state of the art is summarized in the paper by Givehchi and Tan [16]. We choose the latest one for each of these two mechanisms. The single fiber efficiency for neutral particles in a slip flow for a Brownian diffusion (η_D) considering slipping effect is described using the following equation [62].

$$\eta_D = 0.84\text{Pe}^{-0.43} \tag{13.12}$$

where Pe is Peclet number is defined using Eq. (13.13)

$$\text{Pe} = \frac{U_0 d_f}{D_p} \tag{13.13}$$

The single fiber filtration efficiency for interception mechanism η_{it} is [41]

$$\eta_{\text{it}} = 0.6\left(\frac{1-\alpha}{Y}\right)\frac{R^2}{1+R}\left(1+\frac{1.996\text{Kn}_f}{R}\right) \tag{13.14}$$

Y is the Kuwabara hydrodynamic factor, defined using Eq. (13.15). It is a function of filter solidity α

$$Y = -\frac{\ln\alpha}{2} - \frac{3}{4} + \alpha - \frac{\alpha^2}{4} \quad \text{for } \text{Kn}_f \ll 1 \tag{13.15}$$

Kn_f is the fiber Knudesn number described in Eq. (13.16)

$$\text{Kn}_f = 2\lambda/d_f \tag{13.16}$$

where d_f is the fiber diameter and R is the interception parameter defined in Eq. (13.17).

$$R = \frac{d_p}{d_f} \tag{13.17}$$

Example 13.1: Nanoaerosol filtration efficiency
A filter is made of fiberglass with a solidity of 5 %, and it is 5-cm thick. The average diameter of the fibers is 5 μm. When the face speed is 0.15 m/s, calculate and plot the fractional transport efficiency as a function of particle aerodynamic diameter in the range of 1–100 nm under standard conditions, by interception and diffusion, respectively.

Solution
In this problem, the following parameters are considered as constant

$$d_f = 5\,\mu\text{m}, \alpha = 0.05, \mu = 1.81 \times 10^{-5}\,\text{Pa.s}$$

$$\text{Kn}_f = \frac{2\lambda}{d_f} = 0.0264$$

$$Y = -\frac{\ln\alpha}{2} - \frac{3}{4} + \alpha - \frac{\alpha^2}{4} = 0.80$$

The following variables can be calculated in an Excel sheet for different particle diameters

$$R = \frac{d_p}{d_f}$$

$$C_c = 1 + \mathrm{Kn}_p \left[1.142 + 0.558 \exp\left(-\frac{0.999}{\mathrm{Kn}_p} \right) \right]$$

$$D_p = \frac{kTC_c}{3\pi\mu d_p}$$

$$\mathrm{Pe} = \frac{U_0 d_f}{D_p}$$

The single fiber filtration efficiency by inertial interception and diffusion, per unit length of fiber is calculated using

$$\eta_{\mathrm{it}} = 0.6 \left(\frac{1-\alpha}{Y} \right) \frac{R^2}{1+R} \left(1 + \frac{1.996 \mathrm{Kn}_f}{R} \right)$$

$$\eta_D = 0.84 \mathrm{Pe}^{-0.43}$$

With the face speed of 0.15 m/s, we can get the single mechanism filtration efficiency for interception, and diffusion. The result is shown in Fig. 13.3.

As seen in Fig. 13.3, diffusion dominates the nanoaerosol particle transport. The transport efficiency by diffusion increases from nearly 0 to 100 % as the particle size decreases from 100 to 1 nm.

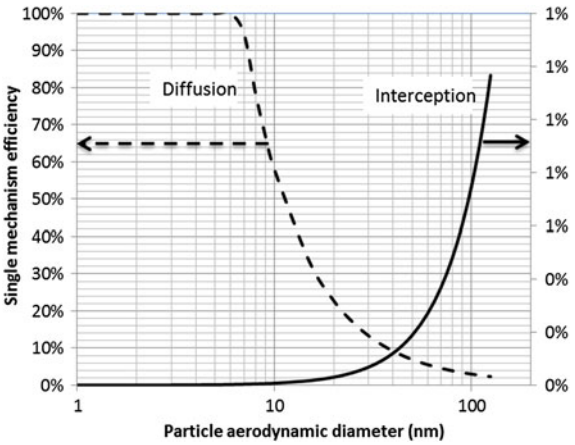

Fig. 13.3 Calculated nanoaerosol filtration efficiency

13.4.2 Adhesion Efficiency and Nanoaerosol Thermal Rebound

In conventional filtration theory, the adhesion efficiency is assumed unity ($\eta_{ad} \equiv 1$). However, it is not certain for nanoaerosol particles. Conventional filtration theory (in Sect. 6.5) indicates that nanoaerosol particle filtration efficiency increases inversely with particle size. Base on this hypothesis, filtration efficiency of nanoaerosol particles can reach 100 % for a properly designed filter. In reality, however, there should be a critical size from which filtration efficiency drops with the decrease of particle diameter (see Fig. 13.4). Otherwise, gas molecules, which are indeed extremely small particles, should be captured by filters resulting in no separation of aerosol particles and the carrier gas. Knowledge of this critical size is important to the design of effective nanoaerosol filters.

When an aerosol particle impacts on a filtration surface, there is an interfacial adhesion force attempting to hold them together. When the adhesion force is strong enough to offset the outgoing momentum at the end of impact, the particle is captured by the filtration surface. It has been well accepted that aerosol particles always stick on the surface in contact. However, this may not be true for nanoaerosol particles because the impact between a solid nanoparticle and a solid surface is most likely elastic because of the small contact area, high speed, and unique properties of nanoaerosol [10]. As a result, nanoparticles may rebound from the filtration surface.

Most researchers (e.g., [60]) assume that the thermal speed of nanoaerosol particles follow the Maxwell–Boltzmann distribution, which is described in Eq. (13.18).

$$f(v_{im}) = 4\pi v_{im}^2 \left(\frac{m}{2\pi kT}\right)^{3/2} \exp\left(-\frac{mv_{im}^2}{2kT}\right) \tag{13.18}$$

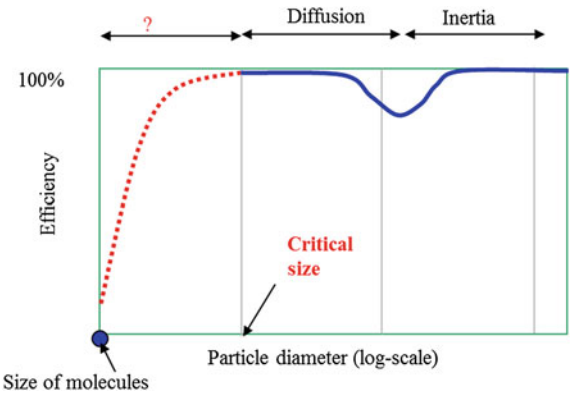

Fig. 13.4 Filtration efficiency vs aerosol particle diameter (not in scale)

where m, k and T denote particle mass, the Boltzmann constant and temperature, respectively. Following the analysis that is similar to the molecular dynamics introduced in Sect. 2.1, the mean impact speed of the nanoaerosol particles is described by Eq. (13.19)

$$\overline{v}_{\text{im}} = \sqrt{\frac{8kT}{\pi m}} \tag{13.19}$$

where the mass (m) in the denominator is now the mass of a single nanoaerosol particle instead of that of a gas molecule. With the mass of a particle, $m = \rho_p \pi d_p^3/6$, Eq. (13.9) becomes

$$\overline{v}_{\text{im}} = \sqrt{\frac{48kT}{\pi^2 \rho_p d_p^3}} \tag{13.20}$$

Equation (13.4) shows that $\overline{v}_{\text{im}} \propto d_p^{-1.5}$. Therefore, the mean thermal impact speed increase dramatically as particle size drops.

We can use Eq. (13.20) to estimate the mean thermal impact speeds of nanoaerosol particles with aerodynamic diameters in the range of 1–100 nm in standard air. For standard air, $T = 293$; particle density $\rho_p = 1{,}000\,\text{Kg}/\text{m}^3$. We can plot the thermal impact speed vs particle diameter in a logarithm scale as in Fig. 13.5.

This assumption may be valid only for dispersed nanoaerosol particles. It has been widely accepted and validated that Maxwell–Boltzmann distribution governs the speed of gas molecules by which the nanoaerosol particles are surrounded, then the motion of the particles are resulted from the impact between the gas molecules and the aerosol particles. The nanoaerosol particles may not move as freely and randomly as the gas molecules due to their inertia. Unlike gas molecules, which do not coagulate to each other upon collision, nanoaerosol particles could agglomerate

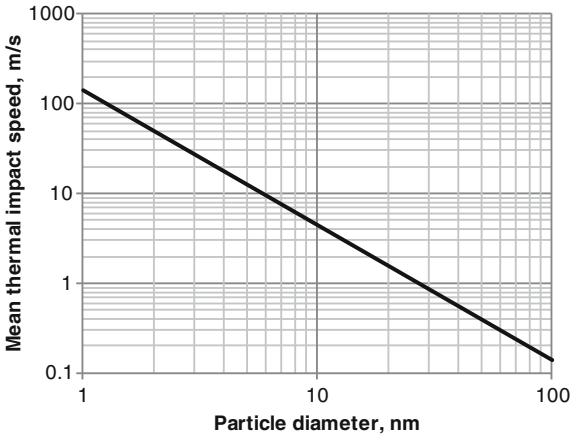

Fig. 13.5 Thermal impact speed of nanoaerosol particle in standard air

and change in size and number concentration. Thus, the assumption of Maxwell–Boltzmann distribution of nanoparticle thermal speed might be valid for diluted cases only. Nonetheless, we have to carry on with the analysis before a better hypothesis is established.

13.4.3 Critical Thermal Speed

The critical particle speed that enables thermal rebound of aerosol particles is a function of adhesion energy (E_{ad}), the coefficient of restitution (e) and particle mass (m).

$$v_{cr} = \sqrt{\frac{2E_{ad}}{me^2}} \tag{13.21}$$

The particle critical velocity, above which particle rebounds from the surface, is calculated using Eq. (13.21) and, with $m = \rho_p \pi d_p^3/6$, it becomes

$$v_{cr} = \sqrt{\frac{12E_{ad}}{\left(\pi \rho_p d_p^3\right)e^2}} \tag{13.22}$$

where E_{ad} is the adhesion energy, which will be elaborated shortly, e is the coefficient of restitution defined as the particle velocity at rebound over the normal particle velocity at the instant of contact. While intuitively one may assume that $e \approx 1$ for nanoaerosol because of the great rigidity, it is not true. The absolute value is unknown [16]. The coefficient of restitution is dependent on the material of the nanoparticles and the filter surface and the impact velocity of the nanoparticles [3]. For the impact velocities close to the critical velocity, the coefficient of restitution is small, and it leads to small rebound velocities. Molecular dynamics simulation by Ayesh et al. [3] showed that, for solid nanoparticles,

$$e \leq 0.6$$

Unfortunately, the database for coefficient of restitution for nanoparticles is still not well developed yet.

13.4.4 Adhesion Efficiency

Since the particles are considered as being collected when their thermal velocities are below v_{cr}, the fractional adhension efficiency can be mathematically described by

$$\eta_{ad} = \frac{\int_0^{v_{cr}} f(v_{im})\mathrm{d}v_{im}}{\int_0^{\infty} f(v_{im})\mathrm{d}v_{im}} \tag{13.23}$$

With the assumption of Maxwell–Boltzmann distribution for the particle thermal/impact velocity, Eq. (13.23) can be written as, by cancelling the common constants

$$\eta_{ad} = \frac{\int_0^{v_{cr}} v_{im}^2 \exp\left(-\frac{mv_{im}^2}{2KT}\right)\mathrm{d}v_{im}}{\int_0^{\infty} v_{im}^2 \exp\left(-\frac{mv_{im}^2}{2KT}\right)\mathrm{d}v_{im}} \tag{13.24}$$

Note that the general integration of

$$\int \left[x^2 \exp\left(-ax^2\right)\right]\mathrm{d}x = \frac{\sqrt{\pi}\mathrm{erf}(\sqrt{a}x)}{4a^{1.5}} - \frac{x \times \exp(-ax^2)}{2a} \tag{13.25}$$

where erf is the error function, and erf(0) = 0; erf(∞) = 1. And $x\Delta\exp(-ax^2) \rightarrow 0$ when $x \rightarrow \infty$, the numerator and the denominator in Eq. (13.24) are, respectively,

$$\int_0^{v_{cr}} v_{im}^2 \exp\left(-\frac{mv_{im}^2}{2KT}\right)\mathrm{d}v_{im} = \frac{\sqrt{\pi}\mathrm{erf}\left(\sqrt{\frac{m}{2KT}}x\right)}{4\left(\frac{m}{2KT}\right)^{1.5}} - \frac{x\exp\left(-\frac{m}{2KT}x^2\right)}{\frac{m}{KT}} \tag{13.26}$$

$$\int_0^{\infty} v_{im}^2 \exp\left(-\frac{mv_{im}^2}{2KT}\right)\mathrm{d}v_{im} = \frac{\sqrt{\pi}}{4\left(\frac{m}{2KT}\right)^{1.5}} \tag{13.27}$$

Then the adhesion efficiency can be described as

$$\eta_{ad} = \mathrm{erf}\left(\sqrt{\frac{m}{2KT}}v_{cr}\right) - \sqrt{\frac{2m}{\pi KT}}v_{cr} \cdot \exp\left(-\frac{m}{2KT}v_{cr}^2\right) \tag{13.28}$$

Recall that

$$\overline{v}_{im} = \sqrt{\frac{8kT}{\pi m}} \tag{13.29}$$

Equation (13.28) becomes

$$\eta_{ad} = \text{erf}\left(\frac{2}{\sqrt{\pi}}\frac{v_{cr}}{\overline{v}_{im}}\right) - \frac{4}{\pi}\frac{v_{cr}}{\overline{v}_{im}}\exp\left[-\frac{4}{\pi}\left(\frac{v_{cr}}{\overline{v}_{im}}\right)^2\right] \tag{13.30}$$

For the ease of presentation, we define an interim term

$$z = \frac{2}{\sqrt{\pi}}\frac{v_{cr}}{\overline{v}_{im}} \tag{13.31}$$

The equation for adhesion energy can be simply presented as

$$\eta_{ad} = \text{erf}(z) - \frac{2z}{\sqrt{\pi}}\exp\left[-z^2\right] \tag{13.32}$$

For the ease of calculation without software, the error function can be approximated with

$$\text{erf}(z) \approx 1 - \frac{1}{\left(1 + a_1 z + a_2 z^2 + a_3 z^3 + a_4 z^4\right)^4} \tag{13.33}$$

where a_1 = 0.278393, a_2 = 0.230389, a_3 = 0.000972, and a_4 = 0.078108. The maximum error is 5×10^{-4} (Fortran 77 manual).

13.4.5 Adhesion Energy

Several models of adhesion energy (E_{ad}) were developed before and they were summarized by Givehchi and Tan [16]. As guidance, we will introduce only two of them, the JKR model [24] and the DMT model [11]. These two models complement each other because they represent two extremes in the Tabor parameter spectrum. JKR model is applicable to soft material, large radius, compliant spheres, and large adhesion energy and DMT model is for hard material, small radius with low adhesion energy [33]. The effectiveness of the DMT model has been proven for smaller and stiffer contact solids [44]. However, the main defect in this theory is that it neglects deformations outside the contact area [33].

Consider a nanoparticle deformed on the solid surface in Fig. 13.6. The adhesion energy between the particles and the surface of the filter material can be mathematically calculated based on consideration of elastic or plastic impaction.

$$E_{ad} = \Delta\gamma\pi a^2 \tag{13.34}$$

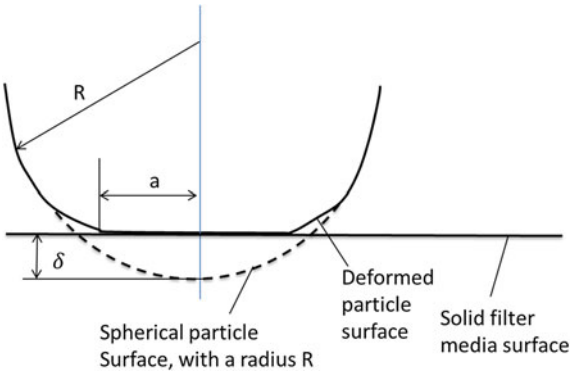

Fig. 13.6 Schematic diagram of adhension energy analysis

where $a =$ the contact radius between particle and filter fiber and πa^2 is the contact area, E_{ad} = the adhesion energy (J), $\Delta\gamma =$ the specific adhesion energy (J/m^2), and $\Delta\gamma$ is a function of the Hamaker constant [11].

$$\Delta\gamma = \frac{H}{12\pi Z_e^2} \tag{13.35}$$

where Z_e = 0.4 nm is the equilibrium distance between the bodies. $H =$ the Hamaker constant between the particle and the filter surface. A great deal of uncertainty is thus related to the determination of the specific adhesion energy especially in the case of nanomaterials.

The Hamaker constant between the particle and the filter surface can be calculated using

$$H = \left(H_p H_f\right)^{1/2} \tag{13.36}$$

Table 13.2 Material properties for thermal rebound calculation

Material	Hamaker constant $H_i \times 10^{19}$ J	Density (kg/m^3)	Mechanical constant $\left(K_i \times 10^{11}\ \mathrm{m}^2/\mathrm{N}\right)$	
			Calculated by Givehchi [16]	Given by Wang and Kasper [60]
Polystyrene	0.79	1,005	10.130	8.86
Glass (Dry)	0.85	2,180	0.443	–
NaCl	0.7	2,165	0.746	2.35
WOx (Tungsten)	1.216	19,250	0.071	–
Steel	2.12	7,840	0.137	0.139
Nickle			–	0.137
Copper	3.3	8,890	0.218	0.216
Fused quartz	0.65		–	0.432

where the subscript p and f stand for particle and filter surface, respectively. A typical Hamaker constant is in the order of (10^{-19}–10^{-21}) J. The values for some materials are listed in Table 13.2.

Example 13.2: Specific adhesion energy
Estimate the specific adhesion energy between a NaCl particle and a glass fiber

Solution
For salt particles and a glass fiber filter, $H_p = 7 \times 10^{-20}$ J, $H_f = 8.5 \times 10^{-20}$ J; then the Hamaker constant is

$$H = \left(H_p H_f\right)^{1/2} = \sqrt{7 \times 8.5} \times 10^{-20}\,\mathrm{J} = 7.71 \times 10^{-20}\,\mathrm{J}$$

The specific adhesion energy is

$$\Delta\gamma = \frac{H}{12\pi Z_e^2} = \frac{7.71 \times 10^{-20}\,\mathrm{J}}{12\pi(0.4 \times 10^{-9})^2\,\mathrm{m}^2} = 0.0128\,\mathrm{J/m}^2$$

where $Z_e = 0.4$ nm.

By considering the effect of surface adhesion energy and contact pressure inside the contact area, the contact radius between bodies and the adhesion energy are respectively given by the following two equations, ignoring the external force:

$$\begin{cases} a = \left[\dfrac{R^*}{Y^*}\left(6\Delta\gamma\pi R^*\right)\right]^{1/3} & \text{(JKR Model)} \\ a = \left[\dfrac{R^*}{Y^*}\left(2\Delta\gamma\pi R^*\right)\right]^{1/3} & \text{(DMT Model)} \end{cases} \tag{13.37}$$

where R^* = the characteristic radius of two bodies. In this case, they are considered as the nanoaerosol particle and the filter fiber. And it is defined as

$$\frac{1}{2R^*} = \frac{1}{d_p} + \frac{1}{d_f} \tag{13.38}$$

Y^* is the composite Young's modulus of bodies with the mechanical constant of K_P and K_f

$$Y^* = \frac{4}{3\pi}\left(\frac{1}{K_p + K_f}\right) \tag{13.39}$$

Mechanical constants are also listed in Table 13.2.

Example 13.3: Nanoaerosol adhesion efficiency
Calculate the adhesion efficiency using the DMT model with the following

properties of a glass fiber filter for NaCl nanoparticles 1–100 nm when filter fiber diameter $d_f = 5\,\mu\text{m}$.

Solution
For salt particles and glass fiber filter

$$H_p = 7 \times 10^{-20}\,\text{J}$$

$$H_f = 8.5 \times 10^{-20}\,\text{J}$$

$$K_p = 0.75 \times 10^{-11}\,\frac{\text{m}^2}{\text{N}}$$

$$K_f = 0.443 \times 10^{-11}\,\frac{\text{m}^2}{\text{N}}$$

Then the Hamaker constant

$$H = \left(H_p H_f\right)^{1/2} = \sqrt{7 \times 8.5} \times 10^{-20} J = 7.71 \times 10^{-20}\,\text{J}$$

And the specific adhesion energy is

$$\Delta\gamma = \frac{A_H}{12\pi Z_e^2} = \frac{7.71 \times 10^{-20}\,\text{J}}{12\pi(0.4 \times 10^{-9})^2\,\text{m}^2} = 0.0128\,\text{J}/\text{m}^2$$

The composite Young's modulus of bodies with the mechanical constants of K_p and K_f

$$\begin{aligned} Y^* &= \frac{4}{3\pi}\left(\frac{1}{K_p + K_f}\right) = \frac{4}{3\pi}\left(\frac{1}{0.75 \times 10^{-11} + 0.443 \times 10^{-11}}\right) \\ &= 3.51 \times 10^{11}(Pa) \end{aligned}$$

The characteristic radius of two bodies is

$$R^* = \frac{1}{2}\left(\frac{1}{d_p} + \frac{1}{d_f}\right)^{-1}$$

The impact contact area is determined by

$$a = \left[\frac{R^*}{Y^*}(2\Delta\gamma\pi R^*)\right]^{1/3}$$

Then the adhesion energy is calculated using

$$E_{\text{ad}} = \Delta\gamma\pi a^2$$

Then the critical speed and impact speed are calculated using

$$v_{\text{cr}} = \sqrt{\frac{12E_{\text{ad}}}{\pi\rho_p d_p^3 e^2}}; \quad \overline{v}_{\text{im}} = \sqrt{\frac{48kT}{\pi^2\rho_p d_p^3}}$$

Then the adhesion efficiency is determined by

$$z = \frac{2}{\sqrt{\pi}}\frac{v_{\text{cr}}}{\overline{v}_{\text{im}}}; \quad \eta_{\text{ad}} = \text{erf}(z) - \frac{2z}{\sqrt{\pi}}\exp\left[-z^2\right]$$

In calculation using spread sheet, the error function is approximated with

$$\text{erf}(z) \approx 1 - \frac{1}{\left(1 + a_1 z + a_2 z^2 + a_3 z^3 + a_4 z^4\right)^4}$$

where a_1 = 0.278393, a_2 = 0.230389, a_3 = 0.000972, and a_4 = 0.078108.

The results are shown in Fig. 13.7 in terms of penetration efficiency.

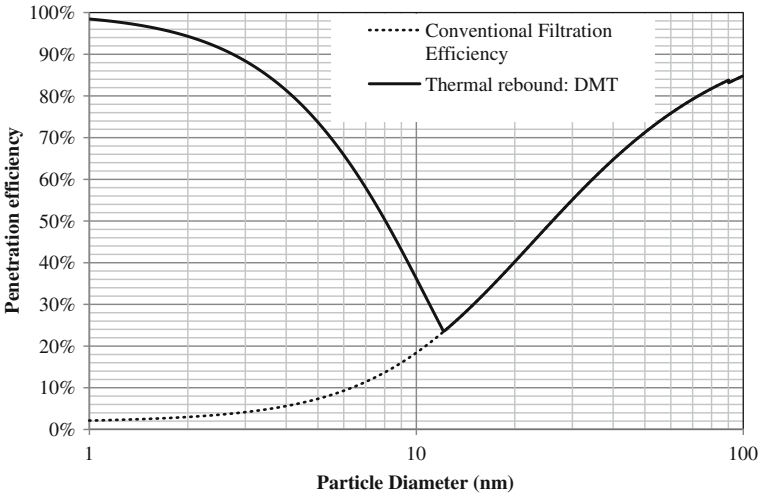

Fig. 13.7 Calculated penetration efficiency using DMT model

13.5 Nanoaerosol Characterization

Nanoaerosol can be sampled on a filter or grid for offline analyses of the morphology and composition of individual particles. The most common offline method is transmission electron microscope (TEM) and energy-dispersive X-ray spectroscopy (EDX). However, the physical and chemical properties may change due to agglomeration and/or chemical reactions during the sampling, transport and offline characterization processes. An online measurement is preferred when it is available.

Online monitoring of nanoaerosol is applied mainly to measure the size distribution. A number of technologies have been developed to measure airborne nanoparticle size distribution for use in a laboratory setting. And they are briefly summarized for guidance as follows.

13.5.1 Scanning Mobility Particle Sizer

Scanning mobility particle sizer (SMPS) employs a differential mobility analyzer (DMA) to classify nanoaerosols based on their electrical mobility after passing through a bipolar charger; the performance of a DMA is mostly limited by the low charging efficiency of sub-20 nm nanoaerosol particles. Classified nanoparticles are sent into a condensation particle counter (CPC), where they grow to 25 μm by condensation in butanol or water vapor. Then these large particles are counted by light scattering technique.

The principles of SMPS were introduced by Wang and Flagan [59]. Particles of different sizes are separated in DMA based on their electrical mobilities that depend on particle size. The electrical mobility Z_p, a measure of the particle's ability to move in an electric field, is defined as

$$Z_p = \frac{neC_c}{3\pi\mu d_p}. \tag{13.40}$$

where n is number of elementary charges on the particle, e is the charge of an ion, C_c is the Cunningham slip correction factor, μ is gas viscosity and d_p is particle diameter.

The polydisperse aerosol enters a bipolar neutralizer in the electrostatic classifier where aerosol particles reach a state of charge equilibrium due to collisions with bipolar ions. Then the charged aerosol enters DMA. The DMA consists of two concentric metal cylinders. The inner cylinder (r_1) is maintained at a controlled negative DC voltage and outer one (r_2) is electrically grounded. Thus, an electric field between the two cylinders is created. The polydisperse aerosol (flow rate Q_p) and sheath air (flow rate Q_{sh}) from the top of the classifier flow down the annular space between the cylinders. Due to the action of the electric field, positively charged particles are attached to the inner electrode while negatively charged

particles are attached to the outward one. Uncharged particles are removed with the excess flow. Only particles with the optimum electrical mobility Z_p^* exit the DMA, and

$$Z_p^* = \frac{Q_{\text{sh}}}{2\pi \overline{V} L} \ln\left(\frac{r_2}{r_1}\right) \tag{13.41}$$

where Q_{sh} is sheath air flow rate (equal to excess air flow rate), r_2 is outer radius of annular space, r_1 is inner radius of annular space, $\overline{V}$ is average voltage on the inner collector rod, L is length between the exit slit and polydisperse aerosol inlet.

Combining Eqs. (13.40) and (13.41) leads to the particle diameter measured as a function of the collector rod voltage, number of charges on the particle, classifier flow rate, and geometry of the DMA:

$$d_p = \frac{2(ne)\overline{V} L C_c}{3\mu Q_{\text{sh}} \ln\left(\frac{r_2}{r_1}\right)} \tag{13.42}$$

By changing the voltage supplied to the inner cylinder of the DMA, scanning over the whole particle size interval is possible.

Once the particles are classified according to electrical mobility; their number concentration is measured by CPC. The CPC counts particles with a diameter from a few nanometers to one micrometer. It is very difficult to optically detect submicron particles because they have a diameter that is comparable with or even less than the wavelengths of most lights. To address this challenge, CPC works by passing the aerosol samples though a supersaturated vapor stream; the vapor condenses quickly on the nanosized particles. These large droplets with nanoparticles as seeds inside can be easily detected or counted by optical methods. The pulses of scattered light are collected by a photo detector and converted into electrical pulses. The concentration of particles is obtained from calibration of DC voltage against known concentrations.

The combination of size and number gives us the particle size distribution. To obtain this particle size distribution SMPS requires about 2 min.

13.5.2 Particle Classification by Aerodynamic Particle Focusing

Alternatively, particle can be classified by aerodynamic particle focusing. Under normal condition, nanoaerosol particle follow the air due to its noncontinuum behavior. As introduced in Sect. 4.2.4 above, the inertia of a particle in curvilinear motion is characterized by the Stokes number (Stk), which is defined in Eq. (13.43).

$$\mathrm{Stk} = \frac{\tau U_0}{d_c} = \frac{\rho_p d_p^2 C_c U_0}{18\mu d_c} \tag{13.43}$$

where the characteristic dimension d_c in the above equation depends on the specific application. U_0 is the undisturbed air velocity. In standard air, a particle with Stk $\gg$ 1.0 will continue in a straight line as the fluid turns around the obstacle. But for Stk $\ll$ 1, particles will follow the fluid streamlines closely.

Example 13.4: Stokes numbers of nanoaerosol particles
Estimate the Stokes numbers of nanoaerosol particles with an aerodynamic particle diameter of 100 nm in standard air flowing at 1 m/s perpendicular to a cylinder of diameter 1 cm.

Solution
Given U_0 = 1 m/s, d_c = 1 cm, $\rho_p = 1{,}000$ kg/m^3, and $d_p = 100$ nm

Under standard conditions

$$Kn = 2\lambda/d_p = 2 \times 66/100 = 1.32$$

$$C_c = 1 + Kn\left[1.142 + 0.558\ \exp\left(-\frac{0.999}{Kn}\right)\right]$$
$$= 1 + 1.32\left[1.142 + 0.558\ \exp\left(-\frac{0.999}{1.32}\right)\right] = 4.36$$

$$\mathrm{Stk} = \frac{\rho_p d_p^2 C_c U_0}{18\mu d_c} = \frac{1000 \times (100 \times 10^{-9})^2 \times 4.36 \times 1}{18 \times 1.81 \times 10^{-5} \times 0.01} = 1.34 \times 10^{-5}$$

The extremely small Stokes number indicates that nanoparticles follow air under STD conditions and it is difficult to separate them from the air simply by inertia. However, it is doable under other conditions when the particle viscosity is reduced and the particle Cunningham correction factor is enhanced. Under a carefully engineered condition with low pressure, however, nanoaerosol particles can be separated from the gas phase because of the relatively small amount of molecules surrounding the nanoaerosol particles.

By this approach, nanoaerosol particles can then be focused to a beam after expansion through an orifice, referred to as aerodynamic particle focusing. Aerodynamic focusing of particles has been employed for the accurate particle sizing [13]. As depicted in Fig. 13.8, the trajectories of the aerosol particles depend on their corresponding *Stokes* number. A well designed focusing orifice could isolate particles down to a few nanometers [42]. Large particles cross the center line due to

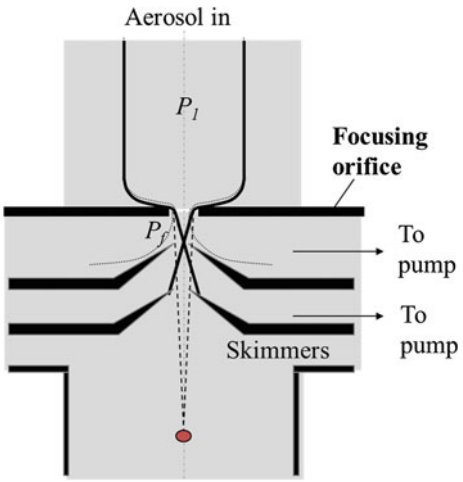

Fig. 13.8 Schematic diagram of aerodynamic partile focusing

great inertia and small ones with low inertia do not cross the center line. The optimally focused particle size by a focusing orifice can be described as [31, 36]

$$d_p^* = \sqrt{\left(d_p^m\right)^2 + (1.657\lambda)^2} - 1.657\lambda \tag{13.44}$$

where λ is the mean free path of the carrier gas, the maximum size of the focused particles (d_p^m) is a function of critical Stokes number Stk^*,

$$d_p^m = \frac{18\mu d_f \mathrm{Stk}^*}{\rho_p v_f} \tag{13.45}$$

where ρ_p is the density of particle, μ is the viscosity of gas, d_f is the focusing orifice diameter and v_f is the average speed in the focusing orifice exit plane. Gas speed in the focusing orifice should reach sonic speed to enable aerodynamic focusing of a certain-size particle. The critical Stokes number Stk^* is based on the gas properties at the orifice throat. The value of Stk^* has been numerically determined to be between 1 and 2 [31] and experimentally determined to be around 2 [42]. It does not depend on the pressure of the carrier gas.

Substituting Eq. (13.45) into (13.44) leads to

$$d_p^* = \sqrt{\left(\frac{18\mu d_f \mathrm{Stk}^*}{\rho_p v_f}\right)^2 + (1.657\lambda)^2} - 1.657\lambda \tag{13.46}$$

This equation shows that the optimally focused particle size d_p^* depends on the properties of the gas such as the mean free path (λ) and viscosity (μ) of the carrier gas and the focusing orifice diameter (d_f) the gas viscosity and the gas velocity through

the orifice. From an engineering practice point of view, it is challenging to alter the diameter of the focusing orifice or the gas velocity through the orifice. However it is doable to control the size of the optimally focused particles by changing the gas mean free path, which can be done by adjusting the upstream gas pressure.

The optimally focused size also depends on the location of the measurement spot downstream the focusing orifice [13]. For each pressure setting, the focusing is defined by the mean particle size (d_p^*) and the range of particle sizes focused (Δd_p^*).

13.5.3 Particle Counting by Current Measurement Electrospray Technique

Aerosol particles can be counted by relating their diameters to the maximum charges of ions. According to what we learned in Sect. 6.3.2, the maximum amount of ions a particle can carry is a function of particle diameter. For nanoaerosol particles, diffusion charging is the dominating mechanism, and the number of ions can be estimated by

$$n(t) = \frac{d_p kT}{2e^2 K_E} \ln\left(1 + \frac{d_p K_E \bar{c}_i \pi e^2 N_{i0}}{2kT} t\right) \tag{13.47}$$

The current by these moving particles with charges is

$$I = N_p Q n e \tag{13.48}$$

This current can be detected by a Faraday cup connected to an electrometer. By combination of aerodynamic particle focusing and current measurement, we can measure the particle size distribution of nanoaerosol particles [54, 56].

The electrometers for the detection of nanosized aerosol particles must be extremely sensitive. The GRIMM model 5.705 electrometer can measure the charge on aerosol particles of the size 0.8–700 nm. Another option is the TSI 3068B electrometer, which measures total net charge on aerosol particles from 2 nm to 5 μm.

Due to the unique properties of nanoaerosol, too much is unknown in this emerging area of research. Unfortunately, there is still a great need to develop stationary or portable instrument to measure particle size distribution that are practical for broad industrial applications.

Online chemical characterization of nanoaerosol is another challenge with significant potential for future research. Compared to size distribution instruments, much less is developed for online analysis of nanoaerosol chemical composition. No instrumentation has been reported aiming at online single particle chemical analysis for sub-10 nm nanoaerosols, which is crucially needed in order to fully understand the mechanisms of secondary aerosol nanoaerosol formation [6]. Currently, it has to be conducted by a combination of offline and online approaches in a statistically significant manner.

13.6 Nanoaerosol Generation

Nanoaerosol particle instruments are calibrated by suppliers or specialized laboratories before they are delivered to end users. In addition to the primary and secondary calibration methods, calibration shall also include a check on the particle number counters's (PNC's) detection efficiency with particles of a known size, often being 23 nm (electrical mobility diameter). Proper selection of the test aerosol particles is essential to the PNC calibration [15]. However, PNCs from different manufacturers are calibrated using different aerosol materials. For example, emery oil from TSI and NaCl from GRIMM. When they are used for industrial nanoaerosol, such as diesel soot, a material with similar behavior with diesel soot should be used too for the calibration.

An ideal aerosol generator is expected to be able to produce a constant and reproducible output of stable aerosol particles with adjustable size and concentration distributions. There are many nanoaerosol generators developed and commercially available based on different mechanisms. Typical ones are summarized as follows.

13.6.1 Evaporation–Condensation Technique

This method can be used for the generation of solid nanoaerosol particles like NaCl, C40 (tetracontane), silver or Tungsten. Nanoparticles are produced based on the principle of evaporation and condensation on nuclei. As shown in Fig. 13.9, the bulk nanoaerosol material is placed in a ceramic crucible (shown) or a ceramic heater container (not shown), where the bulk material is heated to its boiling point. A small flow is introduced into the heater, above the bulk material, to displace the concentrated vapor. The hot vapor is delivered to an area where it is mixed with the cool carrier air to enable condensation.

The output is polydisperse nanoaerosol where particles can be as small as 2 nm [46], which is the starting point of nucleation [29]. The nanoaerosol particle sizes can be varied by controlling one or both of the following factors.

- the crucible air flow rate (to control the vapor feeding rate)
- the carrier air flow (to control the subsequent cooling rate).

13.6.2 Electrospray Technique

This method is employed mainly for the generation of nanosized liquid droplets. As shown in Fig. 13.10, the bulk liquid material (e.g., Emery 3004 or PAO 4 cSt) is feed through a capillary into a container or suspended through a capillary tube from the container. By applying an electrical field to liquid at the capillary tip, the liquid

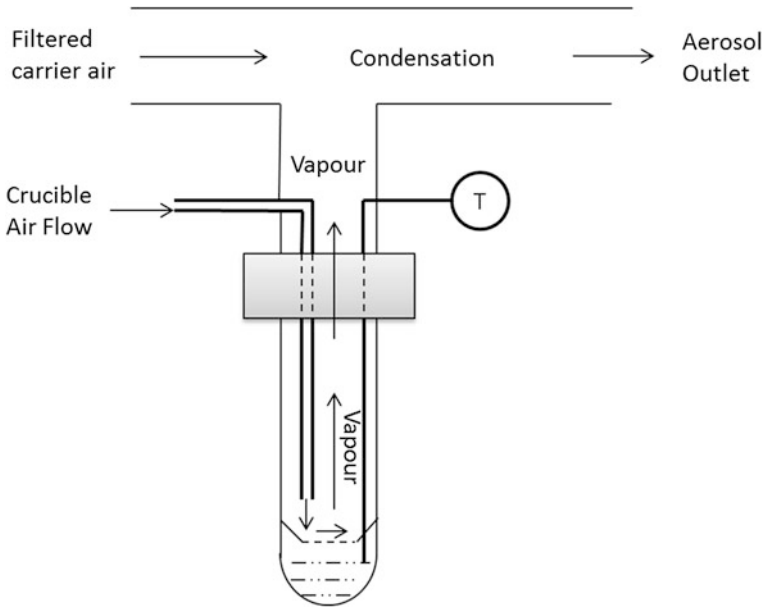

Fig. 13.9 Evaporation–condensation technique for nanoaerosol generation [15]

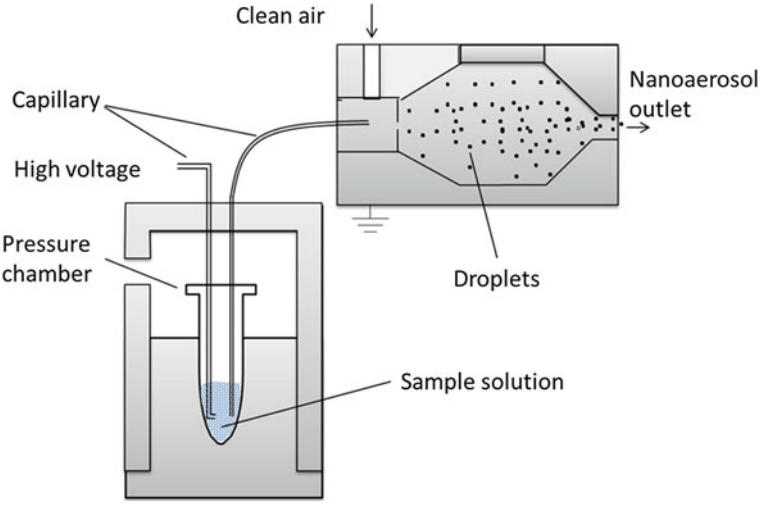

Fig. 13.10 Electrospray technique for nanoaerosol generation [15]

is drawn from the tip into a conical jet to mix with the clean air to produce nanoaerosol. These nanoparticles are then neutralized by an ionizer. Meanwhile, Air and CO_2 are merged with the droplets, and the liquid evaporates [15].

The output is neutralized monodisperse aerosol particle that is free of solvent residue. The particles are supposed to be spherical in shape. The sizes can be downs to a few nanometers. The factors that affect the concentration and the size distribution of nanoaerosols include solution concentration, humidity, and pressure. More about this technique can be found in literature (e.g., [37]).

13.6.3 Soot Nanoaerosol Particles

A properly designed combustion process can be used to generate soot particles, and it can also be called a soot generator. A soot generator uses a diffusion flame to form soot particles during pyrolysis (Fig. 13.11). A gaseous fuel is preferred for easy operation. Within the soot generating burner the flame is mixed with quenching gas at a definite flame height, resulting in a soot particle flow. Extra air is introduced then to dilute the soot particle stream.

The output aerosol particle sizes are controlled by means of varying fuel and its flow rate (in the order of ml per minute), air flow rate (e.g., 200 ml/min) and the inert quenching gas (say, Nitrogen) flow rate (e.g., 1 l/min) and further dilution air stream flow rate (1 l/min) [15]. Sufficient quenching ensures that stable soot particle output in terms of size and concentration. The generated aerosol particle diameter can be down to a few nanometers and within a range of 10^6–10^7 particle/cm^3 are diluted by quench gas and as an option, subsequently by adding dilution air.

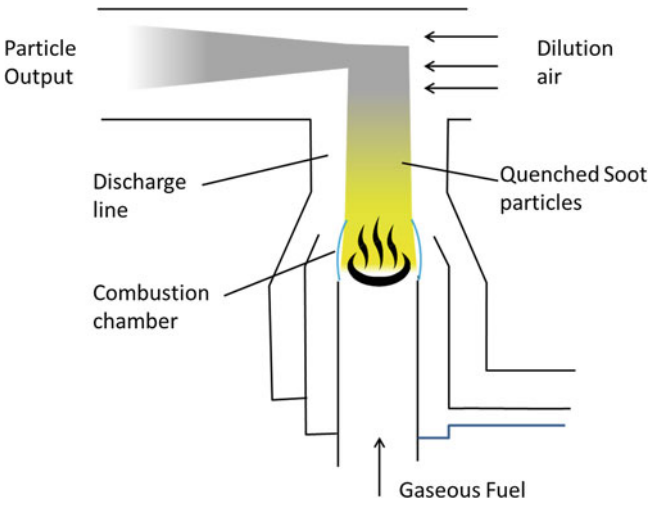

Fig. 13.11 Combustion-based soot particle generation [15]

References and Further Readings

1. Alonso M, Hernandez-Sierra A, Alguacil F (2002) Diffusion charging of aerosol nanoparticles with an excess of bipoloar ions. J Phys A Math Gen 35:6271–6280
2. Anastasio C, Martin S (2001) Atmospheric nanoparticles. In: Banfield JF, Navrotsky A (eds) Nanoparticles and the environment. Reviews in mineralogy & geochemistry 44. Mineralogical Society of America, Chantilly, VA, pp 293–349
3. Ayesh AI, Brown SA, Awasthi A, Hendy SC, Convers PY, Nichol K (2010) Coefficient of restitution for bouncing nanoparticles. Phys Rev B: Condens Matter 81:195422–195426
4. Biris AS, De S, Mazumder MK, Sims RA, Buzatu DA, Mehta R (2004) Corona generation and deposition of metal nanoparticles on conductive surfaces and their effects on the substrate surface texture and chemistry. Part Sci Technol 22:405–416
5. Brun E (ed) (2012) Risk perception and risk communication with regard to nanomaterials in the workplace: European risk observatory literature review, European agency for safety and health at work (EU-OSHA). Publications Office of the European Union, Luxembourg
6. Bzdek B, Pennington M, Johnston M (2012) Single particle chemical analysis of ambient ultrafine aerosol: a review. J Aerosol Sci 52:109–120
7. Castellano P, Ferrante1 R, Curini1 R, Canepari S (2009) An overview of the characterization of occupational exposure to nanoaerosols in workplaces. J Phys Conf Ser 170:012009
8. Chang J, Lawless PA, Yamamoto T (1991) Corona discharge processes. IEEE Trans Plasma Sci 19:1152–1166
9. Cohen B, Xiong J, Fang C, Li W (1998) Deposition of charged particles on lung airways. Health Phys 74:554–560
10. Dahneke B (1971) The capture of aerosol particles by surfaces. J Colloid Interface Sci 37:342–353
11. Derjaguin BV, Muller VM, Toporov YP (1975) Effect of contact deformations on the adhesion of particles. J Colloid Interface Sci 53:314–326
12. Ferin J, Oberdoerster G, Penney DP, Soderholm SC, Gelein R, Piper HC (1990) Increased pulmonary toxicity of ultrafine particles? 1. Particle clearance, translocation, morphology. J Aerosol Sci 21:381–384
13. Fernández de la Mora J, Riesco-Chueca P (1988) Aerodynamic focusing of particles in a carrier gas. J Fluid Mech 195:1–21
14. Ferreira AJ, Cemlyn-Jones J, Cordeiro C (2013) Nanoparticles, nanotechnology and pulmonary nanotoxicology. Pneumologia 19:28–37
15. Giechaskiel B, Alessandrini S, Forni F, Carriero M, Krasenbrink A, Spielvogel J, Gerhart C, Wang X, Horn H, Southgate J, Jörgl H, Winkler G, Jing L, Kasper M (2008) Calibration of PMP condensation particle number counters: effect of material on linearity and counting efficiency, EUR 23495 EN—2008. European Commission Joint Research Centre, Institute for Environment and Sustainability. doi:10.2788/95549, http://ies.jrc.ec.europa.eu/
16. Givehchi R, Tan Z (2014) An overview of airborne nanoparticle filtration and thermal rebound theory. Aerosol Air Qual Res 14:45–63
17. Hakim LF, Portman JL, Casper MD, Weimer AW (2005) Aggregation behavior of nanoparticles in fluidized beds. Powder Technol 160:149–160
18. Hautanen J, Kilpelainen M, Kauppinen EI, Jokiniemi J, Lehtinen K (1995) Electrical agglomeration of aerosol particles in an alternating electric field. Aerosol Sci Technol 22:181–189
19. Hernandez-Sierra A, Alguacil FJ, Alonso M (2003) Unipolar charging of nanometer aerosol particles in a corona ionizer. J Aerosol Sci 34:733–745
20. Hinds W (1999) Aerosol technology: properties, behavior, and measurement of airborne particles, 2nd edn. Wiley-Interscience, NJ
21. Ichitsubo H, Hashimoto T, Alonso M, Kousaka Y (1996) Penetration of ultrafine particles and ion clusters through wire screens. Aerosol Sci Technol 24:119–127

22. Intra P, Tippayawong N (2011) An overview of unipolar charger developments for nanoparticle charging. Aerosol Air Qual Res 11:187–209
23. Jaques P, Kim C (2000) Measurement of total lung deposition of inhaled ultrafine particles in healthy men and women. Inhal Toxicol 12:715–731
24. Johnson L, Kendall K, Roberts A (1971) Surface energy and the contact of elastic solids. Proc R Soc Lond A 324:301–313
25. Jouve G, Goldman A, Goldman M, Haut C (2001) Surface chemistry induced by air corona discharges in a negative glow regime. J Phys D Appl Phys 34:218
26. Kimoto S, Mizota K, Kanamaru M, Okuda H, Okuda D, Adachi M (2009) Aerosol charge neutralization by a mixing-type bipolar charger using corona discharge at high pressure. Aerosol Sci Technol 43:872–880
27. Kittelson DB (1998) Engines and nanoparticles: a review. J Aerosol Sci 29:575–588
28. Kulmala M, Mordas G, Petaja T, Gronholm T, Aalto PP, Vehkamaki H, Hienola AI, Herrmann E, Sipila M, Riipinen I, Manninen HE, Hameri K, Stratmann F, Bilde M, Winkler PM, Birmili W, Wagner PE (2007) The condensation particle counter battery (CPCB): a new tool to investigate the activation properties of nanoparticles. J Aerosol Sci 38:289–304
29. Kulmala M, Riipinen I, Sipilä M, Manninen HE, Petäjä T, Junninen H, Dal Maso M, Mordas G, Mirme A, Vana M, Hirsikko A, Laakso L, Harrison RM, Hanson I, Leung C, Lehtinen KEJ, Kerminen V-M (2007) Toward direct measurement of atmospheric nucleation. Science 318:89–92
30. Liu BYH, Pui DYH, Kinstley WO, Fisher WG (1987) Aerosol charging and neutralization and electrostatic discharge in clean rooms. J Environ Sci 30:42–46
31. Mallina R, Wexler A, Johnston M (1999) High speed particle beam generation: simple focusing mechanisms. J Aerosol Sci 30:719–738
32. Marlow W, Brock J (1975) Calculations of bipolar charging of aerosols. J Colloid Interface Sci 51:23–31
33. Maugis D (2000) Contact, adhesion and rupture of elastic solids. Springer, Berlin
34. McPhee J (2011) The curve of binding energy: a journey into the awesome and alarming world of Theodore B. Taylor. Macmillan, London
35. Medved A, Dorman F, Kaufman SL, Pöcher A (2000) A new corona-based charger for aerosol particles. J Aerosol Sci 31:S616–S617
36. Middha P, Wexler A (2003) Particle focusing characteristics of sonic jets. Aerosol Sci Technol 37:907–915
37. Morozov VN (2011) Generation of biologically active nano-aerosol by an electrospray-neutralization method. J Aerosol Sci 42(5):341–354
38. Mouret G, Chazelet S, Thomas D, Bemer D (2011) Discussion about the thermal rebound of nanoparticles. Sep Purif Technol 78:125–131
39. NIOSH (2005) National Institute for Occupational Safety and Health, NIOSH current intelligence bulletin: evaluation of health hazard and recommendations for occupational exposure to titanium dioxide (2005)
40. Nanocyl (2009) Responsible care and nanomaterials case study nanocyl. Presentation at European responsible care conference, Prague, 21–23 Oct 2009. http://www.cefic.be/Files/Downloads/04_Nanocyl.pdf
41. Payet S, Boulaud D, Madelaine G, Renoux A (1992) Penetration and pressure drop of a HEPA filter during loading with submicron liquid particles. J Aerosol Sci 23:723–735
42. Phares D, Rhoads K, Wexler A (2002) Performance of a single-ultrafine-particle mass spectrometer. Aerosol Sci Technol 36:583–592
43. Pui D, Fruin S, McMurry P (1988) Unipolar diffusion charging of ultrafine aerosols. Aerosol Sci Technol 8:173–187
44. Rahmat M, Ghiasi H, Hubert P (2012) An interaction stress analysis of nanoscale elastic asperity contacts. Nanoscale 4:157–166
45. Romay FJ, Liu BYH, Pui DYH (1994) A sonic jet corona ionizer for electrostatic discharge and aerosol neutralization. Aerosol Sci Technol 20:31–41

46. Scheibel HG, Porstendorfer J (1983) Generation of monodisperse Ag and NaCl aerosols with particle diameters between 2 and 200 nm. J Aerosol Sci 14:113–126
47. Schulte PA, Murashov V, Zumwalde R, Kuempel ED, Geraci CL (2010) Occupational exposure limits for nanomaterials: state of the art. J Nanopart Res 12:1971–1987
48. Seinfeld J, Pandis S (2006) Atmospheric chemistry and physics, Chapter 8. Properties of the atmospheric aerosol, 2nd edn. Wiley-Interscience, Hoboken, pp 350–395
49. Severac C, Jouve G, Goldman A, Goldman M (2004) Chemistry on the low field anodes and cathodes of air corona gaps. J Appl Phys 95:3297–3303
50. Singh Y, Javier JRN, Ehrman SH, Magnusson MH, Deppert K (2002) Approaches to increasing yield in evaporation/condensation nanoparticle generation. J Aerosol Sci 33:1309–1325
51. Stahlmecke B, Wagener S, Asbach C, Kaminski H, Fissan H, Kuhlbusch T (2009) Investigation of airborne nanopowder agglomerate stability in an orifice under various differential pressure conditions. J Nanopart Res 11:1625–1635
52. Stommel YG, Riebel U (2005) A corona-discharge-based aerosol neutralizer designed for use with the SMPS-system. J Electrostat 63:917–921
53. Tabor D (1977) Surface forces and surface interactions. J Colloid Interface Sci 58:2–13
54. Tan Z, Wexler A (2007) Fine particle counting with aerodynamic particle focusing and corona charging. Atmos Environ 41:5271–5279
55. Tan Z (2013) Nanoaerosol. In: Li D (ed) Encyclopedia of microfluidics and nanofluidics, 2nd edn. Springer, New York
56. Tan Z, Givehchi R, Saprykina A (2014) Submicron particle sizing by aerodynamic dynamic focusing and electrical charge measurement, Particuology. doi:10.1016/j.partic.2014.01.002
57. Toyama T, Matsuda H, Ishida I, Tani M, Kitaba S, Sano S, Katayama I (2008) A case of toxic epidermal necrolysis-like dermatitis evolving from contact dermatitis of the hands associated with exposure to dendrimers. Contact Dermat 59(2):122–123
58. Tsai C, White D, Rodriguez H, Munoz C, Huang C, Tsai C, Barry C, Ellenbecker M (2012) Exposure assessment and engineering control strategies for airborne nanoparticles: an application to emissions from nanocomposite compounding processes. J Nanopart Res 14:989
59. Wang SC, Flagan RC (1990) Scanning electrical mobility spectrometer. Aerosol Sci Technol 13:230–240
60. Wang H, Kasper G (1991) Filtration efficiency of nanometer-size aerosol particles. J Aerosol Sci 22:31–41
61. Wang J, Pui DYH (2011) Characterization, exposure measurement and control for nanoscale particles in workplaces and on the road. J Phys Conf Ser 304. doi:10.1088/1742-6596/304/1/012008
62. Wang J, Chen DR, Pui DYH (2007) Modeling of filtration efficiency of nanoparticles in standard filter media. J Nanopart Res 9:109–115
63. White H (1951) Particle charging in electrostatic precipitation. Trans Am Inst Electr Eng 70:1186–1191
64. Zhang L, Ranade MB, Gentry JW (2002) Synthesis of nanophase silver particles using an aerosol reactor. J Aerosol Sci 33:1559–1575